CROSS-SHORE SEDIMENT TRANSPORT: A FIELD TEST OF THE BAILARD ENERGETICS MODEL.

Troels Aagaard[1], Brian Greenwood[2] and Jørgen Nielsen[1].

ABSTRACT: This paper reports on the results from a field test of the Bailard energetics sediment transport model. Model predictions agreed well with observed and measured volumetric change in the inner surf zone under erosional as well as accretionary conditions, occurring over a 72 h long storm event. The observed formation of a nearshore bar was reproduced by the model; bar formation was predicted to be due to a sediment transport convergence generated by seaward directed undertow and landward directed incident wave asymmetry.

INTRODUCTION

Attempts to model cross-shore sediment transport and profile evolution under varying energy conditions has been a major concern within coastal science and engineering and a fairly large number of sediment transport/morphodynamic models exist (e.g. Roelvink and Brøker, 1993). These models have generally been tested using laboratory data as sufficiently detailed high-quality field data are scarce.

An exeption to this has been the energetics model (Bagnold, 1966) and derivations thereof (Bowen, 1980; Bailard, 1981). The Bailard model which uses measured velocity moments as input has been tested in the field by e.g. Guza and Thornton (1985), Russell et al. (1995), Thornton et al. (1996) and Gallagher et al. (1998).

This model generally predicts offshore sediment transport events fairly well; these events occur as a response to mean currents and low-frequency waves during high-energy conditions. Onshore directed transport due to incident waves associated with beach recovery is generally poorly reproduced by the model (Russell et al., 1995; Thornton et al., 1996). A major reason is that the model does not consider phase-changes between velocity and sediment concentration which occur during oscillatory wave motions over

[1]Institute of Geography, University of Copenhagen, Øster Voldgade 10, DK-1350 Copenhagen K., Denmark. e-mail: taa@geogr.ku.dk.

[2]Scarborough College Coastal Research Group, The University of Toronto at Scarborough, 1265 Military Trail, Scarborough Ontario M1C 1A4, Canada.

a rippled bed; ripples mainly occur during low and moderate energy conditions.

In this paper, we test the Bailard energetics model using a data set which was collected during a 3½-day moderate storm event at Skallingen on the Danish North Sea coast. During this event, the inner nearshore was subjected to fairly large morphological changes involving an initial onshore bar migration followed by renewed bar formation and finally onshore migration of the newly formed bar. The model was capable of reproducing these morphological changes. Model predictions are also compared quantitatively with measured volumetric changes as well as with suspended sediment flux which was measured during the event.

THE MODEL

Predicted sediment transport was computed from the Bailard-model following the methodology of Thornton et al. (1996), where cross-shore sediment transport is predicted by

$$\langle q_x(t)\rangle = K_b(\langle |u_t|^2 u'\rangle + \langle |u_t|^2 \bar{u}\rangle) - K_{bg}\langle |u_t|^3\rangle + K_s(\langle |u_t|^3 u'\rangle + \langle |u_t|^3 \bar{u}\rangle) - K_{sg}\langle |u_t|^5\rangle \quad (1)$$

where

$$u_t = (u'^2+v'^2+\bar{u}^2+\bar{v}^2+2(u'\bar{u}+v'\bar{v}))^{1/2} \quad (2)$$

and

$K_b = (\rho/\rho_s-\rho)c_f g a'(e_b/\tan\phi);$
$K_{bg} = K_b(\tan\beta/\tan\phi);$
$K_s = (\rho/\rho_s-\rho)c_f g a'(e_s/w_s);$
$K_{sg} = K_s(e_s/w_s)\tan\beta$

$\bar{u},\bar{v}$ are the mean cross-shore and longshore velocities, respectively, u',v' are the oscillatory cross-shore and longshore velocity components, β is beach slope, w_s is sediment fall velocity and $\tan\phi$ the angle of repose; a' is the pore space factor = 0.6. The bedload and suspended load efficiency factors e_b, e_s were set at 0.21, 0.025 (Bailard, 1981). c_f was determined from $c_f = f_w/2$ with $f_w = \exp(5.213(k_s/A)^{.194}-5.977)$, where bed roughness k_s was set to $5D_{50}$ for a flat mobile bed and A is the oscillatory velocity amplitude; $A = u_{max}T/2\pi$ with T being the peak spectral density. c_f was on the order of 0.003-0.004 depending upon location within the profile. These parameters were kept constant at all times; no further adjustments were undertaken.

In eq.(1), the first two terms are the bedload transport terms due to oscillatory and mean cross-shore currents, respectively; terms four and five are the corresponding suspended load terms while the final two terms are due to gravity. u' was further subdivided into incident wave and infragravity wave components using Fourier-filtering.

THE FIELD EXPERIMENT

The field experiment was conducted during October 1995 in the shallow inner surf zone

at Skallingen. Four instrument stations, termed S1-S4, spanned the inner nearshore bar and two additional stations (S5-S6) were deployed on the beach and only submerged during high tides and/or storm surges (Figure 1). The instrument stations were each equipped with one Marsh-McBirney OEM512 electromagnetic current meter, initially installed at 0.23-0.34 m above the bed and vertically adjusted at each low tide (if possible) to compensate for bed level changes. The sensors were oriented to record positive flows landward and to the north; errors in orientation are estimated to be within +/- 3 degrees. Sensor offsets which were on the order of < 0.02 m/s were removed prior to data analysis while sensor gains were computed according to the manufacturer's specifications.

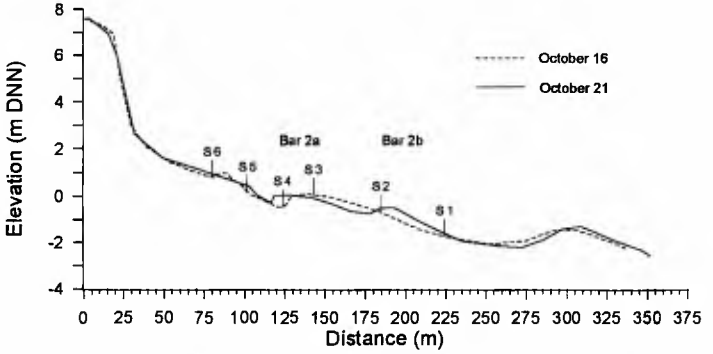

Figure 1. The cross-shore profile of the instrument transect surveyed prior to (Oct.16) and after (Oct.21) the storm event. Locations of the instrument stations as well as bar designations are indicated.

The stations were also each equipped with 3 OBS 1-P optical backscatter sensors (installed at nominal elevations of 0.05, 0.10 and 0.20 m above the bed) while pressure sensors were deployed at S1 and S5. All sensors were sampled at 4 Hz for periods of 34 minutes each 1-1½ hours during the event.

Bed elevation and hence morphological changes were recorded at each low tide through the experiment using a cross-shore array of twenty-eight ½-inch steel rods, spaced at 5 m increments along the instrument transect from x=50-185 m (Figures 1 and 2). The distance from the top of the rods to the sand was measured using a graduated rod fitted with an endplate. As the bed was always flat and tightly packed at low tide, survey errors were small and estimated as +/- 0.5 cm. Potential cumulative errors across the survey section are thus +/- 0.7 m^3/m.

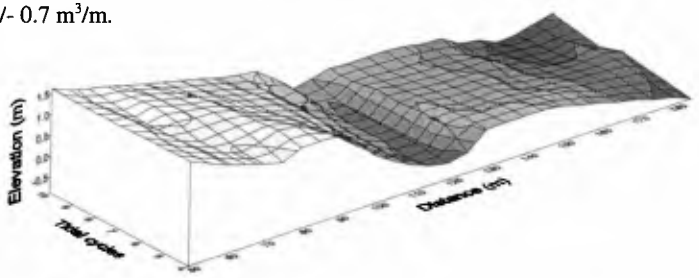

Figure 2. Time-distance diagram of the morphological evolution of the beach/inner surf zone during the experiment (tidal cycles 5-10). Note the trough formation at x = 170 m and the onshore migration of bar 2b into the survey area during tidal cycle 10.

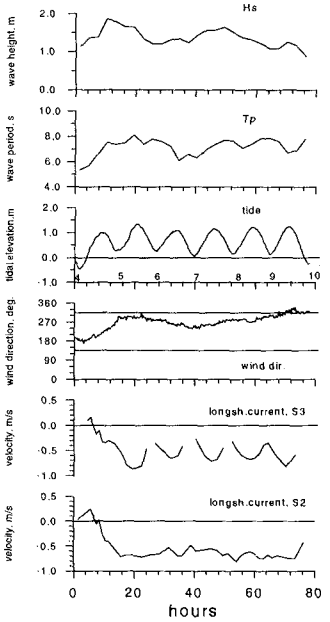

Figure 3. Offshore wave characteristics, tidal elevation, wind direction and longshore current velocities during the storm event. Negative longshore currents are directed to the south.

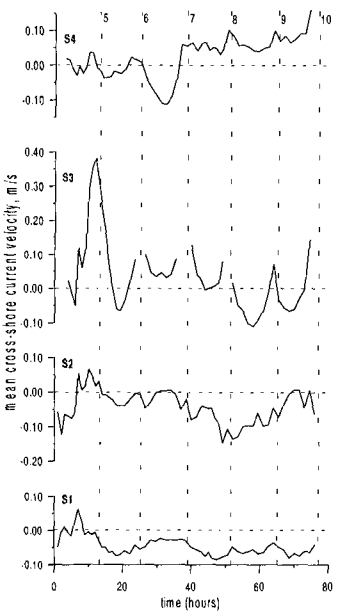

Figure 4. Mean cross-shore current velocities measured at S1-S4. The vertical dashed lines indicate times of low tide. Onshore currents are positive.

The storm event was characterized by moderate wave energy with a maximum significant wave height of H_s = 1.9 m seaward of the surf zone (Figure 3). Depending upon tidal stage, waves broke between stations S1 and S2. Wave periods were 7-8 seconds and the winds which were oblique to the shoreline generated relatively strong southward directed longshore currents, on the order of 0.7-0.9 m/s. The longshore currents were tidally modulated with maximum currents occurring at high tide when local wave energy level (radiation stress) was at a maximum.

Measured cross-shore mean currents were initially directed landward across the nearshore bar (Figure 4). At this time, cross-shore currents at the bar crest (S3) were also tidally modulated but in this case with maximum currents at low tide when incident wave dissipation was large and the breaking waves assumed a roller-like shape. Also, the sensors were relatively higher in the water column. Current velocities reached +0.38 m/s at the bar crest, and these landward directed flows are interpreted as being due to onshore wave- and bore-induced mass transports forming the onshore-directed limb of a rip circulation cell feeding the rip current south of the instrument transect (Aagaard et al., 1998). During the second half of the event, cross-shore currents at S3 (and S2) as well as the tidal modulation of these currents reversed; at this time the maximum currents at S3 occurred at high tide with velocities on the order of -0.05-0.1 m/s. The rip circulation was locally replaced by an undertow (Aagaard et al., 1998).

RESULTS AND DISCUSSION

Bed elevation changes in the beach/inner surf zone region are shown in Figures 2 and 5. The morphological evolution can be separated into three phases: Initially, the inner nearshore bar (bar 2a) migrated onshore during tidal cycles 5-7. Sediment was eroded from the crest of the bar and deposited in the trough and on the beach face. The second phase somewhat overlapped the first (tidal cycles 7-9) and was associated with trough excavation on the seaward slope of the bar (around x = 170 m) with renewed bar formation (bar 2b) seaward of the survey area (Figure 1). The final phase occurred during cycle 10 and was associated with onshore transport of sediment. The inner trough infilled and bar 2b migrated into the survey area. In plan view, the inner bar was initially slightly convex to the shoreline, with the instrument transect (located at y = 0 m) crossing the highest point of the bar (Figure 6). At the termination of the event, bar 2a had merged with the shoreline slightly updrift of the instrument transect and it was oriented obliquely to the shore. Note that the rip channels located at y = +/- 175 m (Figure 6) remained stable in position. The main areas of erosion/accretion were located at the updrift and downdrift ends of the bars.

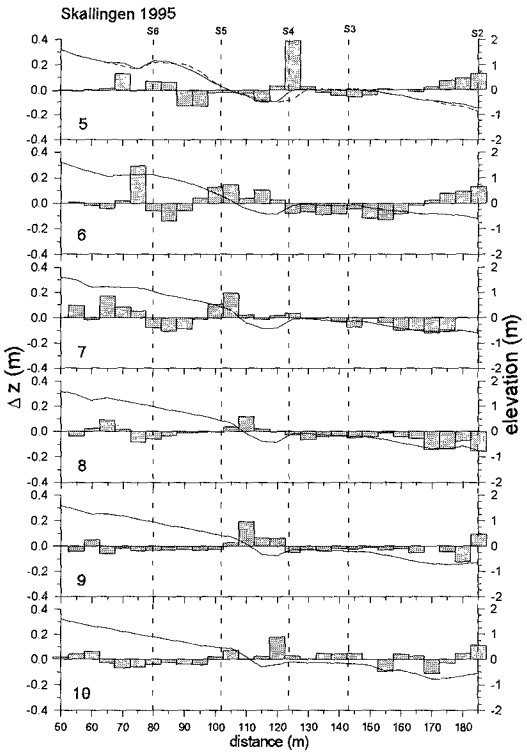

Figure 5. Changes in bed elevation at survey rods (Δz), and the cross-shore profile over tidal cycles 5-10. The left-hand ordinate refers to Δz, while the one on the right refers to elevation above Ordnance Datum. The dashed line in the upper panel is the profile at the termination of tidal cycle 4.

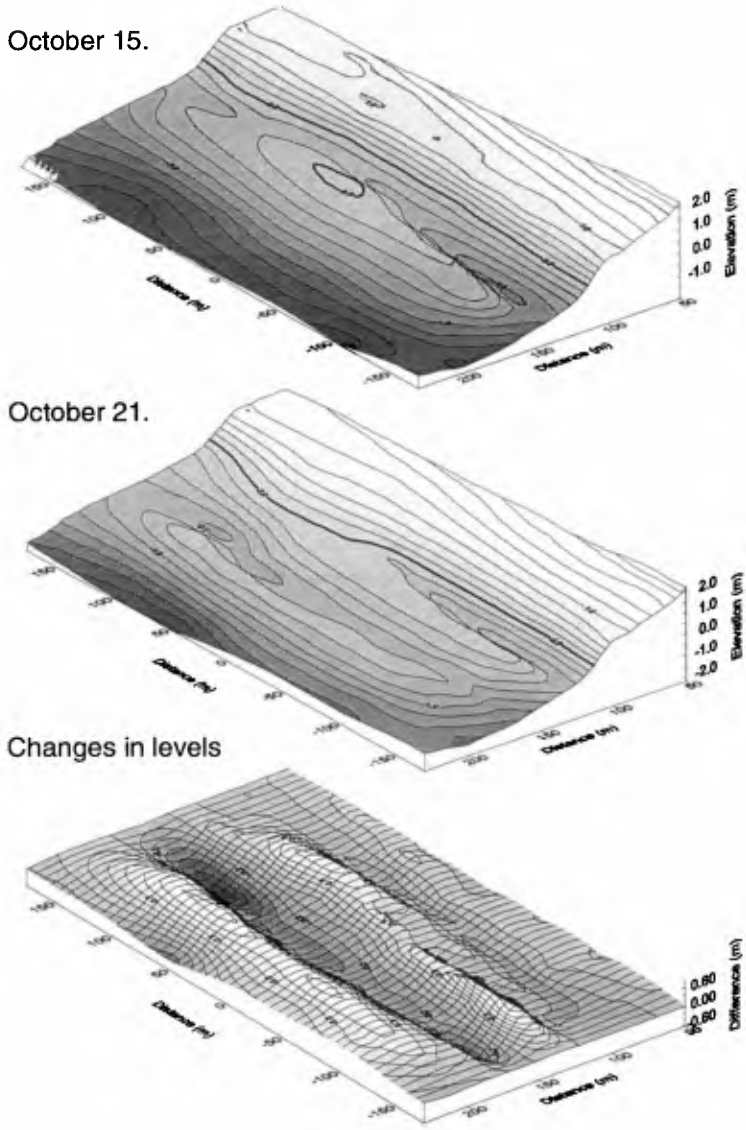

Figure 6. Three-dimensional views of the topography at the field site prior to (October 15) and after (October 21) the storm event. The bottom graph shows positive and negative bed elevation changes. The instrument transect was located at y = 0 m.

Predicted sediment transport

Figure 7 shows model-predicted sediment transport rate at stations S1-S4. Computed sediment transport rates and directions are in qualitative agreement with the observed morphological changes. During cycles 5-7, sediment transport was directed landward at all stations; transports at S4 were, however, very small as this station was located in the trough where sediment concentrations were small due to decreasing incident wave energy. During cycles 7-9, a transport divergence existed between S2 and S3 corresponding to the trough formation at this location. Simultaneously, there was a transport convergence between S1 and S2 resulting in the formation of bar 2b. Finally, tidal cycle 10 was characterized by a reversal to the initial transport conditions with onshore transport across the bar(s). Transport rates at S4 gradually increased as bar 2a migrated through this station and sediment concentrations increased. According to the model, suspended load was significantly more important than bedload, on average ranging from a high of 88% of the total load at S2 where incident wave energy was at a maximum, to 68% at S4.

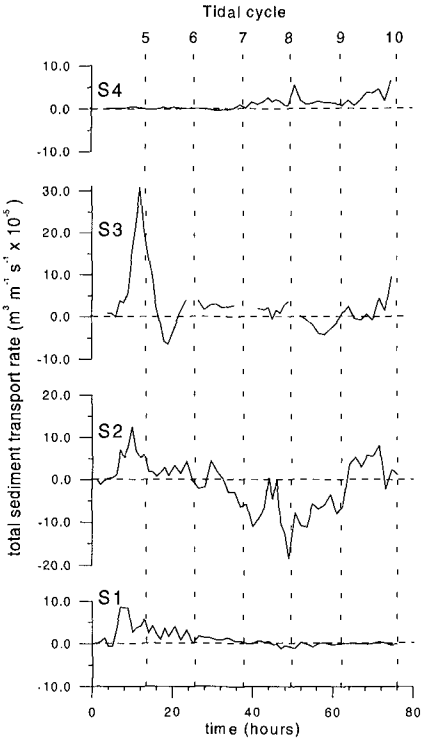

Figure 7. Predicted sediment transport rates at stations S1-S4. Vertical dashed lines indicate times of low tide. Positive values signify onshore directed transport.

Bed elevation changes at the inner edge of the survey area were almost consistently nil (Figure 5). Assuming a closed landward boundary to the profile and assuming a lack of longshore sediment transport gradients (which appears not unreasonable; Figure 6), net volumetric change within the survey area should match the sediment transport rate at the seaward edge of the area, i.e. at S2. In Table 1, predicted net volumetric transport at S2 over individual tidal cycles (ΔQ) is compared with volumetric change landward of S2 (ΔV). In the table, the agreement between predicted and measured volumetric change was excellent in 4 out of 6 cases. During cycles 6 and 9, the model overpredicted the volumetric transport by a factor of 1.7 and 2.4, respectively, resulting in a factor 2 overprediction of the sediment loss over the entire event. Examining the patterns of cut and fill (Figure 6), it is not evident that the overprediction should be mainly due to longshore sediment transport gradients.

Table 1 also compares the sediment balance over bar 2a (bounded by S2 and S4) with predicted sediment transport balance between these two stations. In this case, the correlation was excellent in 3 cases. During cycles 6 and 7, the model underpredicted the loss from the section, associated with onshore sediment transport at S4. This was at least

partly due to the current meter at S4 being very close to the bed (< 0.1 m) as the bar migrated onshore and almost buried this station. The model again overpredicted the sediment loss during cycle 9.

	S2-beach		S2-S4	
Tidal cycle no.	ΔV	ΔQ	ΔV	ΔQ
5	+1.85	+1.79	+1.55	+1.71
6	+0.48	+0.82	-2.09	+0.77
7	-0.56	-0.52	-2.79	-0.50
8	-3.74	-3.78	-3.95	-4.36
9	-1.51	-3.62	-1.78	-4.48
10	+1.65	+1.71	+0.44	+0.36
Total	-1.83	-3.60	-8.62	-6.50

Table 1. Volumetric change (ΔV) between S2 and the most landward survey rod, and between stations S2 and S4, as well as predicted net sediment transport (ΔQ) onshore/into (+) and offshore/out of (-) these sections. Values are in m^3/m shoreline.

Predicted transport vs. measured flux.

Predicted suspended sediment transport rates at S2 and S3 were compared with the sediment flux measurements using the backscatter sensors (Figure 8). Net sediment flux was estimated from these sensors by linearly integrating individual flux estimates from (nominal) elevations z = 0.025-0.275 m. True elevations changed when the bed eroded/accreted. Obviously, such a comparison can not validate quantitatively any of the two methods; a large part of the suspended sediment transport is expected to occur at elevations below the lowermost OBS-sensor and the concentration profiles are not linear. Nevertheless, within the inner surf zone where bores predominate, vertical sediment concentration gradients are expected to be relatively small due to the high levels of turbulence (Yu et al., 1993). Therefore, it should be possible to assess the qualitative performance of the two methods relative to each other.

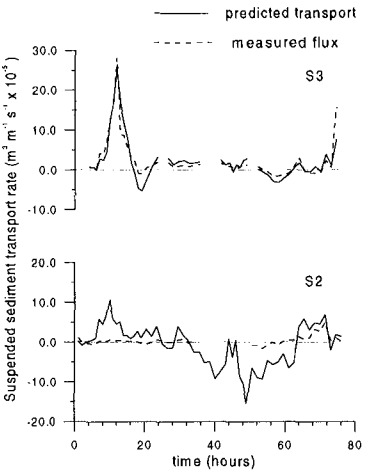

Figure 8. Model-predicted suspended sediment transport versus measured suspended sediment flux at stations S2 and S3. Positive values are directed onshore.

At S3, where measured vertical sediment concentration gradients were generally small, the correspondance between the predicted transport and the measured flux was very good. Data gaps at this station indicate instrument exposure; at S2 the gap represents a period when the OBS-sensors became dislodged and buried. At S2, measured vertical sediment concentration gradients were generally quite large and the correspondance between predicted transport and measured flux was poor except towards the end of the event.

The discrepancy between these stations may have been due to a number of factors. First, vertical mixing appears to have been stronger at S3. Furthermore, bed elevation changes at this station were relatively small (Figure 5) and the sensors were adjusted vertically at each low tide. This was not the case at S2 where bed elevation changes were larger and it was difficult to access this station at low tide. E.g. when the sensors were reinstalled around hour 50 (Figure 8), they could not be deployed sufficiently close to the bed. At this time, the lowermost sensor was at z ~ 0.12 m. As the bed gradually accreted, the correspondance between measurements and predictions improved significantly.

Sediment transport mechanisms

In Figure 9, the predicted suspended sediment transport has been separated into contributions from mean flows and oscillatory incident and infragravity wave components. The Figure illustrates transport rates at stations S1-S4 on three occasions representing the three morphological stages identified earlier. The first example (hour 10) represents the phase when bar 2a migrated landwards. According to the model, this was mainly accomplished by incident wave asymmetry accompanied by onshore directed mean flows on the bar crest. The second phase (hour 49.5) occurred when a trough was excavated between S2 and S3 and bar 2b formed between S1 and S2. This evolution appears to have been mainly due to the reversal of the mean flows which became offshore directed seaward of S3, representing an undertow. The result was a transport divergence between S3 and S2, and a convergence between S2 and S1. At the latter, mean transport became weak and increasingly opposed by incident wave asymmetry. The final example (hour 72) is taken from the time when both bars migrated onshore. At this stage, mean currents had decreased and consequently, onshore directed incident wave asymmetry dominated the inner surf zone.

Figure 9 illustrates a number of important points. First of all, predicted incident wave transport became offshore directed at S2 during tidal cycles 8 and 9 (represented by hour 49.5). This was not a response to an overall reversed incident-wave asymmetry. During the sample run at hour 49.5, velocity asymmetry at high frequencies (computed from $u^3/(u^2)^{0.5}$ and using high-pass filtered time series) was small (+0.071) but positive, i.e. onshore directed. At the preceding high tide (hour 44) incident wave asymmetry was +0.22. Thus, incident wave asymmetry was tidally modulated as would have been expected as asymmetry has been found to decrease into the surf zone (Thornton and Guza, 1989), and at low tide, S2 was further from the breakpoint. The asymmetry was, however, always onshore directed. The reason for the predicted offshore directed transport at wind wave frequencies was that u_f (Eq. 2) tended to be maximum under incident wave troughs at S2.

The waves were incident north of the shore-normal, generating southerly (negative) longshore currents. Figure 10 shows an example of longshore and high-pass filtered cross-

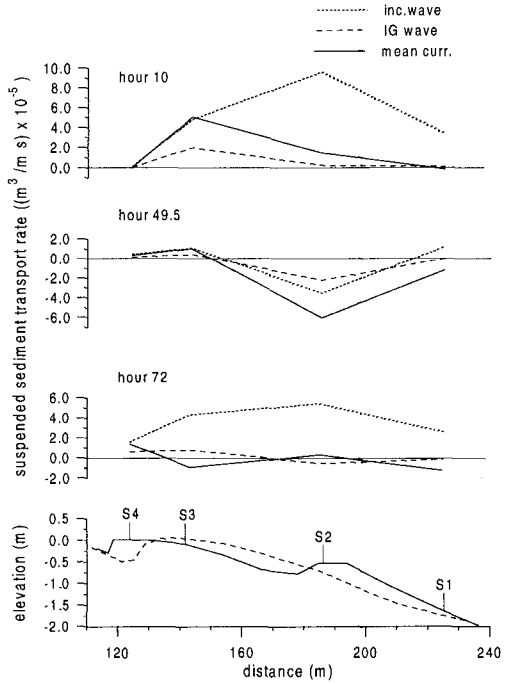

Figure 9. Predicted sediment transport rates due to incident waves (dotted lines), infragravity waves (dashed lines) and mean currents (solid lines) across the nearshore, at representative times. In the lower panel, the dashed line is the profile prior to the storm and the solid line is the profile after the event. Hours 10 and 49.5 represent runs close to low tide whereas hour 72 was a high-tide run.

shore velocity time series at S1 and S2 during hour 49.5. At S1, the velocity field behaved as expected: Maximum onshore velocities occurring under incident wave crests were generally in phase with maximum longshore (southerly) velocities. This was not the case at S2 where the incident waves in many cases appears to have been propagating against the longshore current leading to maximum values of u, in wave troughs. Between S1 and S2, the incident waves appear to have been refracted against the current at this time. The reasons for this are not known, however.

Returning to Figure 9, net sediment transport at oscillatory infragravity wave frequencies tended to be relatively small even though a transport divergence was consistently located between S2 and S3 with onshore directed transport in the innermost surf zone, and more offshore trending transport further seaward.

Finally, as already noted, the mean currents were depth-dependent with respect to directionality. At bar crests (bars 2a and 2b), and particularly at low tide (Figures 4 and 9), the currents were directed onshore while they were directed offshore in larger water depths. This indicates a presence of feed-back mechanisms between topography and mean

current circulation, implying that on gently sloping beaches and in cases when the bar is close to the water surface, e.g. in the intertidal or upper subtidal zones, there will be a tendency towards a generation of rip cell circulation as the water brought onshore by mass

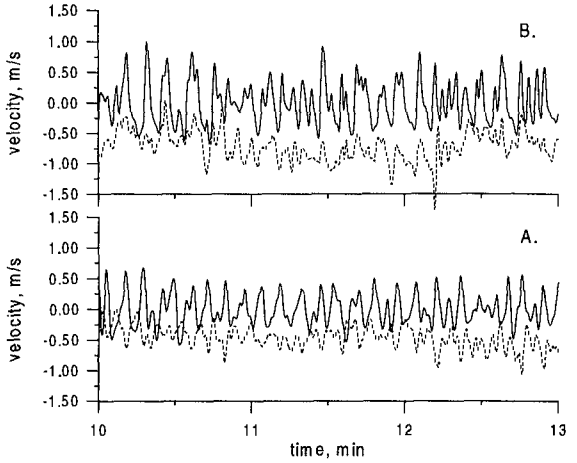

Figure 10. Example time series of longshore velocities (dashed lines) and high-passed cross-shore velocities (solid lines) at stations S1 (A) and S2 (B); runs 292_12 (hour 49.5).

transport cannot escape seaward as an undertow. At Skallingen, rips channels are rarely absent from the inner surf zone.

DISCUSSION AND CONCLUSIONS

In the present study, a vertically homogeneous cross-shore velocity field has been assumed in the sediment transport computations. This might seem inappropriate as most models as well as several laboratory and field studies have demonstrated a tendency for vertically segregated flows, with onshore directed mass transport in the upper part of the water column (generally above trough level) and seaward directed flows in the lower parts. At first glance, the tidally modulated cross-shore current observed at S3 during tidal cycles 5-8 might suggest this scenario as the current sensor was relatively high in the water column at low tide, and vice versa. However, a number of points contradict this interpretation. First, predicted sediment transport rates and directions agreed well qualitatively with the observed volumetric changes, and in most cases quantitatively as well. Second, around low tide rips were visually observed approximately 175 m south (and north) of the instrument transect throughout the event. Third, an undertow did develop at S3 during cycles 9 and 10 (Figure 4) due to reversed longshore pressure gradients (Aagaard et al., 1998). It is not evident why this shift would occur if current direction depended upon sensor elevation as maximum and minimum tidal elevations were relatively constant during all tidal cycles (Figure 3). Finally, the tidally-modulated flow at S2 was far from systematic, suggesting that a simple velocity response to relative sensor elevation did not exist, at least at this station.

Therefore it is concluded that the energetics model is potentially capable of predicting sediment transport rates under high-energy field conditions in the inner surf zone, to within a factor of 2 or 3, provided that longshore velocity components are included in the sediment stirring term. The model appears quite robust as no adjustment of free parameters occurred. On most occasions, there was a close agreement between predicted and measured volumetric change, particularly considering the potential survey errors. While this is probably fortuitous, the model only failed significantly during one tidal cycle.

Previous field tests of the model (e.g. Russell et al., 1995; Thornton et al., 1996) have indicated problems with predicting transport due to incident waves, particularly during onshore sediment transport conditions, and the model has generally been incapable of simulating beach recovery. This was not the case here, probably because the bed in these shallow water depths was generally flat; no evidence of bedforms was observed. The energetics model assumes a zero phase-shift between velocity and sediment concentration; this assumption is violated in the case when the bed is rippled.

The data presented here provide strong support for the concept of nearshore bar formation due to undertow. Approximately half-way through the event, an undertow developed locally at S2 (and later at S3), probably because of reversed longshore pressure gradients (Aagaard et al., 1998). The undertow weakened and became opposed by incident wave asymmetry at S1, resulting in the development of bar 2b.

Finally, this study has suggested an existence of morphodynamic interactions in the nearshore, involving feedbacks between hydrodynamics and topography, exemplified by the dependency between bar topography/water depth and mean flow directions. Apart from the presence or absence of longshore pressure gradients which are intimately linked to longshore (non-)uniform bar topography, the mean flow pattern, i.e. offshore-directed undertow versus onshore-directed rip feeders, seems to be constrained by water depth. In shallow water (bar crests and/or low tide), there was a tendency towards onshore directed mean currents over the bar while offshore directed mean flows prevailed in larger water depths (in troughs, during high tide and at S1).

ACKNOWLEDGEMENTS

This research was supported by the Danish Natural Sciences Research Council, grant no. 11-0925. Superb field assistance was rendered by Ulf Thomas, Rasmus Nielsen, Carlo Sørensen and Torsten Christensen.

REFERENCES

Aagaard, T., Nielsen, J. and Greenwood, B., 1998. Suspended sediment transport and nearshore bar formation on a shallow intermediate-state beach. *Marine Geology*, 148, 203-225.

Bagnold, R.A., 1966. An approach to the sediment transport problem from general physics. *Geological Survey Professional Paper 422-I*. U.S. Government Printing Office, Washington.

Bailard, J.A., 1981. An energetics total load sediment transport model for a plane sloping beach. *Journal of Geophysical Research*, 86, 10938-10954.

Bowen, A.J., 1980. Simple models of nearshore sedimentation; beach profiles and longshore bars. In: S.B.McCann (ed) *The Coastline of Canada*. Geological Survey of Canada, Paper 80-10, 1-11.

Gallagher, E.L., Elgar, S. and Guza, R.T., 1998. Observations of sand bar evolution on a natural beach. *Journal of Geophysical Research*, 103, 3203-3215.

Guza, R.T. and Thornton, E.B., 1985. Velocity moments in nearshore. *Journal of Waterway, Port, Coastal and Ocean Engineering*, ASCE, 111, 235-256.

Roelvink, J.A. and Brøker, I., 1993. Cross-shore profile models. *Coastal Engineering*, 21, 163-191.

Russell, P., Foote, Y. and Huntley, D.A., 1995. An energetics approach to sand transport on beaches. *Proceedings Coastal Dynamics '95*, ASCE, 829-840.

Thornton, E.B., Humiston, R.T. and Birkemeier, W., 1996. Bar/trough generation on a natural beach. *Journal of Geophysical Research*, 101, 12097-12110.

Thornton, E.B. and Guza, R.T., 1989. Wind wave transformation. In: R.J.Seymour (ed) *Nearshore Sediment Transport*, Plenum Press, New York, 137-171.

Yu, Y., Sternberg, R.W. and Beach, R.A., 1993. Kinematics of breaking waves and associated suspended sediment in the nearshore zone. *Continental Shelf Research*, 13, 1219-1242.